



Cite this: *RSC Adv.*, 2019, 9, 34125

# The versatile $\text{Co}^{2+}/\text{Co}^{3+}$ oxidation states in cobalt alumina spinel: how to design strong blue nanometric pigments for color electrophoretic display†

B. Serment,<sup>ab</sup> C. Brochon,<sup>b</sup> G. Hadziioannou,<sup>b</sup> S. Buffière,<sup>a</sup> A. Demourgues<sup>a</sup> and M. Gaudon <sup>\*a</sup>

Blue cobalt inorganic pigments with spinel-type structure have been revisited in order to understand the origin of blackening at low temperatures and to design strong blue nanosized materials. Starting from a sol–gel process, the so-called Pechini route, the correlation between the structural features (inversion rate, Co over-stoichiometry, Co valence states) of the spinel network and its thermal history under air up to high temperatures ( $T = 1400\text{ }^{\circ}\text{C}$ ) allows concluding that the stabilization of  $\text{Co}^{\text{III}}$  in octahedral sites is at the origin of the blackening of the pigment annealed at low and medium temperatures. EELS coupled with TEM analyses (occurrence of multiple phases with various Al/Co atomic ratios) lead to us to conclude definitively about the variation of Co valence states. A top-down (mechanical grinding) and a bottom-up approach lead to the definition of a synthesis route (co-precipitation in basic medium followed by annealing at medium temperatures under Ar) allowing the design of strong blue pure nanosized pigments to be incorporated in inks. Hybrid blue positively charged particles were mixed with white negatively charged particles to formulate dual-colour inks. A dual-colour display was filled with the as-prepared inks and tested under  $\pm 150\text{ V}$ .

Received 15th August 2019  
Accepted 16th October 2019

DOI: 10.1039/c9ra06395a

rsc.li/rsc-advances

## 1. Introduction

Synthetic blue pigments are widely used in the ceramic industry as colouring agents in glazes or porcelain stoneware.<sup>1,2</sup> The first blue modern synthetic pigment, discovered at the beginning of the 18<sup>th</sup> century, was Prussian blue an organic pigment. Through the years, additional inorganic compounds have been added to the spectrum of blue pigments, *e.g.* synthetic ultramarine blue  $\text{Na}_7\text{Al}_6\text{Si}_6\text{O}_{24}\text{S}_3$  and cobalt blue  $\text{CoAl}_2\text{O}_4$ . However, these inorganic pigments needed to be annealed at high temperatures, *i.e.*  $1400\text{ }^{\circ}\text{C}$ , under air in order to get the strongest blue color stabilized in ceramics. The traditional source of the blue colour in ceramic pigments remains the cobalt ion ( $\text{Co}^{2+}$ ),<sup>3</sup> particularly incorporated into spinel networks derived from rock salt and crystallizing in the  $Fd\bar{3}m$  space group. The spinel structure exhibits both octahedral and tetrahedral cationic sites, which lead to large colour scales. Hence, in such frameworks, the crystal field of  $\text{Co}^{2+}$  ( $3d^7$ ) can

increase from 0.5 eV in a tetrahedral environment to 0.8–1.3 eV in a 5-fold or octahedral coordination leading to various d–d transitions on the basis of Tanabe–Sugano diagrams.<sup>4–6</sup> Tetrahedral coordination of  $\text{Co}^{2+}$  is often preferred to octahedral coordination and leads to a strong blue colour in  $\text{CoAl}_2\text{O}_4$  spinel whereas  $\text{Co}^{2+}$  in octahedral coordination is known to exhibit a purple hue.<sup>7</sup> Nevertheless, the colour of  $\text{CoAl}_2\text{O}_4$  pigment can strongly vary depending on the thermal history of the material.<sup>4,7–12</sup> Indeed, the  $\text{CoAl}_2\text{O}_4$  composition (known as Thenard's blue) exhibits an all the more intense sky-blue hue than the annealing temperature is high.<sup>4,7–13</sup> Depending on the pigment thermal history, all the authors<sup>4,7–9,11</sup> have observed that the samples are darker with a greening of the coloration when a low synthesis temperature is applied. These effects can be explained considering various and diverging hypotheses: (i) the occurrence of amorphous carbon, (ii) the presence of a  $\text{Co}_3\text{O}_4$  ( $\text{Co}^{3+}/\text{Co}^{2+}$  mixed valences)/ $\text{Co}_2\text{AlO}_4$  ( $\text{Co}^{3+}$ ) impurity phases with almost similar unit-cell parameter as  $\text{CoAl}_2\text{O}_4$  ( $\text{Co}^{2+}$ ) taking into account the similar ionic radii of  $\text{Co}^{3+}(\text{LS})$  and  $\text{Al}^{3+}$  six-fold coordinated to oxygens,<sup>4,8–11,14–16</sup> (iii) a grain shape influence (taking into account diffusion phenomena)<sup>12,13</sup> or, (iv) the  $\text{Co}^{2+}$  distribution in the network between octahedral and tetrahedral sites.<sup>17–20</sup>

Preliminary works, not reported herein, have dealt with the exploration of several  $\text{CoAl}_2\text{O}_4$  synthesis routes (co-precipitation,

<sup>a</sup>CNRS, Univ. Bordeaux, Bordeaux INP, ICMCB, UMR 5026, F-33600 Pessac, France. E-mail: manuel.gaudon@icmcb.cnrs.fr

<sup>b</sup>CNRS, Univ. Bordeaux, Bordeaux INP, LCPO, UMR 5629, F-33600 Pessac, France

† Electronic supplementary information (ESI) available: Experimental details on synthesis route from inorganic to hybrid particles, TEM images, PXRD patterns, TSI measurements, XPS spectra, Tables with  $\text{CoAl}_2\text{O}_4$  unit-cell parameters and electrophoretic ink parameters. (PDF). See DOI: 10.1039/c9ra06395a



solid state, tartrate, sol-gel and polyol<sup>21</sup>) and their thermal annealing under air or argon (only for the co-precipitation) between 600 °C and 1400 °C. For all the synthesis routes, annealing treatment under air below 1000 °C leads to the obtaining of dark green – black powders whereas blue powders are obtained only for synthesis temperatures above 1200 °C. This paper is focusing on the samples elaborated from sol gel synthesis known as Pechini route where powders have been annealed under air and on oxides prepared from co-precipitation method followed by an argon thermal treatment. The cation distribution and the Co<sup>2+</sup>/Co<sup>3+</sup> oxidation states in the as-prepared CoAl<sub>2</sub>O<sub>4</sub> compounds are characterized and discussed for both synthesis routes. The diffuse reflectance spectra were recorded for all samples/all annealing temperatures and are interpreted in regard of XRD pattern's refinements; Rietveld analysis has been used to calculate the *a* unit-cell parameter, the spinel's inversion factor, and the oxygen atomic coordinate considering various structural hypothesis (the occurrence of one or two phases, the presence of extra Co<sup>3+</sup> substituting for Al<sup>3+</sup>) associated to their reliability factors. EELS and TEM images combined with Energy Dispersive X-ray Spectrometry (EDX) have been also done to investigate in more details the causes of the darkening and greening of the compounds when low synthesis temperatures were used. A complete interpretation of the colour variation of these pigments *versus* the synthesis route and the annealing temperature is thus proposed. Finally, electrophoretic inks have been formulated from these blue pigments and were tested in a prototypal display. For such a demonstration, CoAl<sub>2</sub>O<sub>4</sub> hybrids were mixed with TiO<sub>2</sub> hybrids in a non-aqueous media and a voltage ( $\pm 150$  V) was applied in order to observe the properties of the dual-colour display.

## 2. Experimental

CoAl<sub>2</sub>O<sub>4</sub> pigments were synthesized by a sol gel process: the Pechini route.<sup>22</sup> This chemical process is based on cations chelation by citric acid (CA) and on polyesterification between CA and ethylene glycol (EG) which leads to the formation of a polycationic resin. Aqueous solutions of citrate were prepared by dissolving CA and EG in a minimal volume of water. Then, cationic salts: CoCl<sub>2</sub>·6H<sub>2</sub>O (Alfa Aesar, purity over 98%) and AlCl<sub>3</sub>·6H<sub>2</sub>O (Sigma Aldrich, purity 99%) were added in stoichiometric proportion to the acid solution. A CA-EG/cations molar ratio equal to 4/1 was used. EG-CA polymerization was promoted by removing water with continuous heating on a hot plate. Then, the highly viscous mixtures were thermally treated in two steps: a first calcination at 400 °C under air to remove organics components, then, an annealing step for 10 h between 600 °C and 1400 °C. For the samples being subjected to aggressive ball-milling as post-treatment with the aim to reduce the crystal size, a planetary Fritch pulverisette 7 apparatus was used.

CoAl<sub>2</sub>O<sub>4</sub> pigments were mixed with 10 mL of dried toluene in a 100 mL two-necked flask and then sonicated during 30 minutes. *n*-Octyltrimetoxysilane (OTS) was added to the mixture under magnetic stirring and the flask was heated at 120 °C during 18 hours. The reaction is washed by centrifugation in

toluene and pigments were then dried. Nitroxide Mediated Radical Polymerization (NMRP) *via* dispersion in Isopar G was performed with modified pigments and lauryl acrylate SG1 macroinitiator which were mixed in 10 mL of Isopar G and then sonicated during 1 hour. The solution was outgassed with argon bubbling and monomer was added after 30 min bubbling. The mixture was heated at 120 °C during 19 hours and washed by centrifugation in Isopar G.<sup>23,24</sup>

X-Ray diffraction (XRD) measurements were carried out on a PANalytical X'PERT PRO diffractometer equipped with an X-celerator detector, using Cu(K $\alpha_1$ /K $\alpha_2$ ) radiation with a back filter to avoid the fluorescence of Co ions/atoms when copper source is used. The diffractograms were recorded on 5–120° 2 $\theta$  range with a time per step chosen in order to get 10 000 cps in intensity for the main diffractogram peak. Diffractograms were refined with the Rietveld refinement method using FULLPROF® program package.<sup>25,26</sup> The unit-cell parameters, the atomic positions, the cationic distribution (cation inversion parameter) were then refined (with fixed Debye Waller factors) on the basis of the *Fd3m* space group corresponding to the spinel structure. The peak profiles are fitted with the Caglioti function, *i.e.* considering isotropic crystallites. Uncertainties can be calculated from the standard deviation proposed by the software; these uncertainties being approximated in all cases to the decade higher, all reported results are limited to their last significant digit.

The morphology of CoAl<sub>2</sub>O<sub>4</sub> nanoparticles was roughly evaluated by high resolution transmission electronic microscopy (HRTEM) and STEM has been used for Energy Dispersive X-ray Spectrometry (EDS). High-resolution transmission electronic microscopy (HRTEM) has been performed on TEM Jeol 2200FS operated at 200 kV with a field emission gun. The theoretical resolution (FWHM) was nominally 1.9 Å. The quantification of Co and Al concentrations have been performed by EDS considering K lines intensities and integration. Samples were prepared by dissolving a few milligrams of powder in ethanol directly depositing one drop of the as-prepared suspension on a copper grid. EELS measurements were also carried out with the JEOL 2200 FS transmission electron microscope with an “omega filter” in column and a theoretical energy resolution of 1 eV. The dispersion was chosen at 60  $\mu\text{m eV}^{-1}$  and a comparison of the Co *L*<sub>2,3</sub> edge EELS spectra (at an energy varying between 779 and 794 eV) for various samples and references (CoO, Co<sub>3</sub>O<sub>4</sub>) aim to estimate the average Co valence state.

Hybrid particle morphologies were characterized by transmission electron microscopy (TEM) using JEOL 1400+, at 120 kV with LaB<sub>6</sub> filament and a 0.38 nm resolution. The microscope is equipped with a camera GATAN, with condenser diaphragm.

UV-Vis-NIR diffuse absorbance spectra – presented here after Kubelka–Munk transformation – were recorded at room temperature from 200 to 2500 nm with a step of 1 nm and a band length of 2 nm on a Cary 17 spectrophotometer using an integration sphere. Halon polymer was used as white reference for the blank. A mathematic treatment of the obtained spectra allowed the determination of the *L\*a\*b\** space colorimetric parameters. The first step of the treatment consists in obtaining the XYZ tri-stimulus



values (defined by the CIE, 1964) from the integration (on the visible range, *i.e.* from  $\lambda = 380$  nm up to 780 nm) of the product of  $x(\lambda)$ ,  $y(\lambda)$  or  $z(\lambda)$  functions (CIE – 1964) with the diffuse reflectance spectra function:  $X = \int x(\lambda)R(\lambda)d\lambda$ . Then, the transfer equations defined by the CIE, 1976, from XYZ space to the  $L^*a^*b^*$  space, were used in order to obtain the  $L^*a^*b^*$  chromatic parameters.

The hydrodynamic size and the electrophoretic mobility of colloids were performed by Phase Analysis Light Scattering (PALS) and Dynamic Light Scattering (DLS), using a Nano ZS Malvern Instrument using a wavelength of  $\lambda = 633$  nm and a fixed angle  $\theta = 90^\circ$ . A square shaped wave electric field from 2.5 to 20 kV m<sup>-1</sup> was applied using dip cell designed for measurement in a non-aqueous environment. Each sample was measured 3 times (15 runs per measurement). The  $q$  global charge of hybrid particles was determined using the eqn (1), with  $v$  = the electrophoretic speed (m s<sup>-1</sup>),  $E$ : the applied electrophoretic potential (V);  $R$ : the average radius of the particles;  $g$ : 9.8 m s<sup>-2</sup>;  $\eta$ : the viscosity of the electrophoretic medium in mPa s.

$$v = \frac{\left(qE + \frac{4}{3}\pi R^3 g(\rho_{\text{pig}} - \rho_{\text{pol}})\right)}{6\pi R\eta} \quad (1)$$

Stability of the inks has been estimated using the Turbiscan® lab stability analyser. The analysis of the stability was carried out as a variation of backscattering (BS) and transmittance ( $T$ ) profiles. Eqn (1) is the determination for TSI, compare every scan of a measurement to the previous one, on the selected height, and divide the result by the total selected height in order to obtain a result which is independent of the quantity of sample in the measuring tube.

$$\text{TSI} = \sum_i \frac{\sum_h |T'_{0i}(h) - T'_{0i-1}(h)|}{H} \quad (2)$$

where  $h$  and  $H$  is the selected height and the total height of sample respectively.

### 3. Results and discussion

#### 3.1. CoAl<sub>2</sub>O<sub>4</sub>: black or blue pigments depending on post-annealing treatment

The CoAl<sub>2</sub>O<sub>4</sub> compounds were prepared from Pechini gels annealed under air atmosphere at various temperatures: 600, 800, 1000, 1200 and 1400 °C. The X-ray diffraction patterns of the as-prepared powders are reported in Fig. 1a. On the basis of XRD data, a single spinel phase seems to be obtained whatever the annealing temperature. The narrowing of the peak widths *versus* the increase of the annealing temperature is correlated to a coherent domain increase. Using Debye and Scherrer equation, the crystallite size (coherent domain size) can be approximated from the full width at half maximum of the diffraction peaks (knowing the instrumental broadening). The crystal size was calculated and progressively increases with the annealing temperature, from about 20 nm for the 600°C-annealed compound up to 100 nm for the 1400°C-annealed oxide. UV-

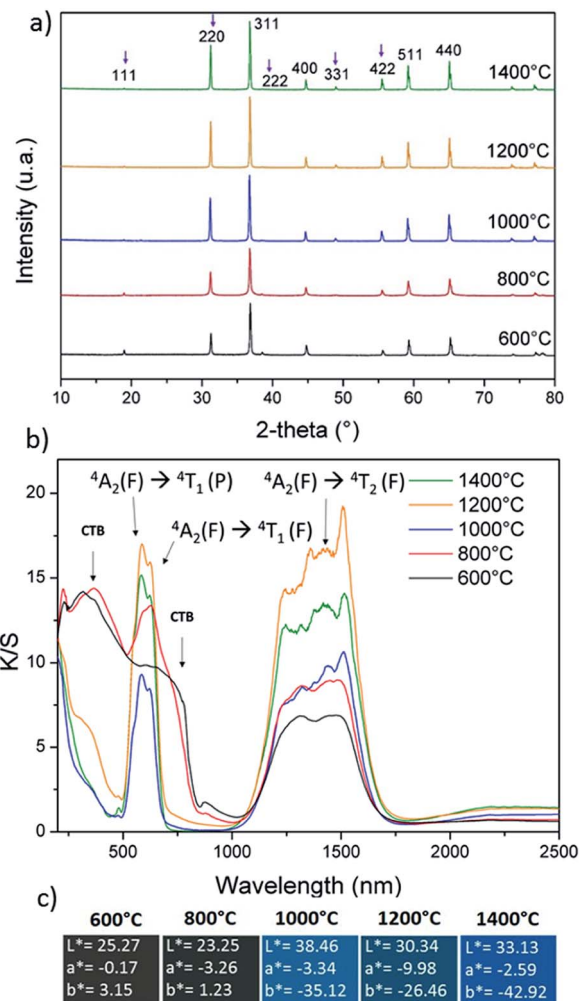


Fig. 1 (a) XRD patterns, (b) K/S spectra and (c)  $L^*a^*b^*$  colour parameters of CoAl<sub>2</sub>O<sub>4</sub> compounds prepared from Pechini route followed by post-annealing at several temperatures.

Vis-NIR absorbance curves (KM transforms) are superimposed for the various as-prepared samples in Fig. 1b. In all cases the d-d transitions associated to the cobalt chromophore in tetrahedral coordination are clearly visible as the  $^4A_2 \rightarrow ^4T_2$  triplet (due to the L-S Russel-Saunders coupling) in NIR range (in between 1150 and 1700 nm) and another multiplet in visible range which can be indexed as the  $^4A_2 \rightarrow ^4T_1$  (P) transition (with an eventual contribution of the  $^4A_2 \rightarrow ^4T_1$  (F) transition). This absorption peak attribution is based on further works reported in literature.<sup>10–12,14–22,25–27</sup> The main triple band in the middle of the visible range was indexed as  $^4A_2 \rightarrow ^4T_1$  (P) transition, which was shown to decompose as a triplet for which the maximal absorptions, for instance in CoAl<sub>2</sub>O<sub>4</sub>, are near 540 nm, 590 nm and 640 nm (ref. 11) and associated to a crystal field around 0.5 eV with a B Racah parameter equal to 750 cm<sup>-1</sup>. Furthermore, in all cases a charge transfer band (CTB) is located at about 350 nm and associated to ligand (oxygen anion) to metal (cobalt and/or aluminium cation) electronic transfer, as awaited for this kind of wide-gap semi-conducting oxide. Nevertheless, the spectra evolve significantly *versus* the annealing





temperature, especially between annealing treatments ranging from 600 °C up to 1000 °C. An additional CTB, being all the more intense that the thermal treatment is performed at low temperature, is associated to another band gap at lower energy around 1.7 eV (roughly 800 nm). Without any doubt, this band is linked to cobalt ions (the unique chromophore ions) which can adopt another oxidation state or are located in various sites (interstitial and/or octahedral sites). This leads to a strong impact on the spinel's coloration and, unfortunately, a significant blackening of the samples prepared at the lowest temperatures.  $L^*$ ,  $a^*$  and  $b^*$  colour parameters were extracted from the diffuse reflectance curves, what allows, after  $L^*a^*b^* \rightarrow$  to RGB colour space transformation, the representation of the colour of each compound with any common software (Fig. 1c). One should have to note the difficulty to obtain highly divided  $\text{CoAl}_2\text{O}_4$  powder with a bright blue colour (nanometric crystal size), a key point for pigments applications which has been reported for long time in the literature.<sup>4,7–9,11</sup> The herein observed blackening is a large subject of matter and the purpose of long debates with interpretations which are diverging depending on the authors. The source of the absorption phenomenon, occurring while spinel compounds are not annealed at sufficiently high temperatures, responsible for the compound blackening, was already attributed to carbon content, the occurrence of CoO or other cobalt-rich impurities or a large inversion rate of the  $\text{Co}^{2+}/\text{Co}^{3+}$  ions inside the spinel structure network (*i.e.* attributed to a significant occupancy of the octahedral sites by the cobalt ions).<sup>16–22,25,26</sup>

TEM investigations on the 600 °C-annealed and the 1000 °C-annealed compounds were performed with the aim to interpret the colour evolution of the as-prepared compounds from nearly black to blue hue *versus* the compound's thermal history. The comparison between the transmission electronic micrographs taken on the two compounds (reported in Fig. 2a) clearly show that, besides the crystal size increase with the annealing treatment, a narrowing of the crystal size distribution also takes place. Indeed, for the 600 °C-annealed compound, nanometric particles are neighbouring with bigger crystals with about 100 nm diameter. On the opposite, the 1000 °C-annealed compound is constituted of submicronic crystals with about 100 nm diameter, which are very homogeneous in terms of size and shape.

EDX analyses were performed on different zones of the 600 °C-annealed sample and on one grain of the 1000 °C-annealed sample (Fig. 2a: zones 1, 2 & 3). This experiment reveals a non-homogeneous cobalt ion distribution, with a positive segregation in the largest crystals to the detriment of the nanometric grains. One can report on the various cobalt and aluminium concentrations extracted from EDX spectra recorded on the zones 1 and 2, for the 600 °C sample (Fig. 2b). However, a homogeneous distribution in the cobalt and aluminium is found on the 1000 °C-annealed sample, furthermore with a Co : Al local ratio in the analysed area (zone 3) which is equal to the global one, *i.e.* Co : Al = 1 : 2 (Fig. 2b).

The occurrence for the 600 °C-annealed compound of a non-uniform cationic distribution is quite surprising in regard of the

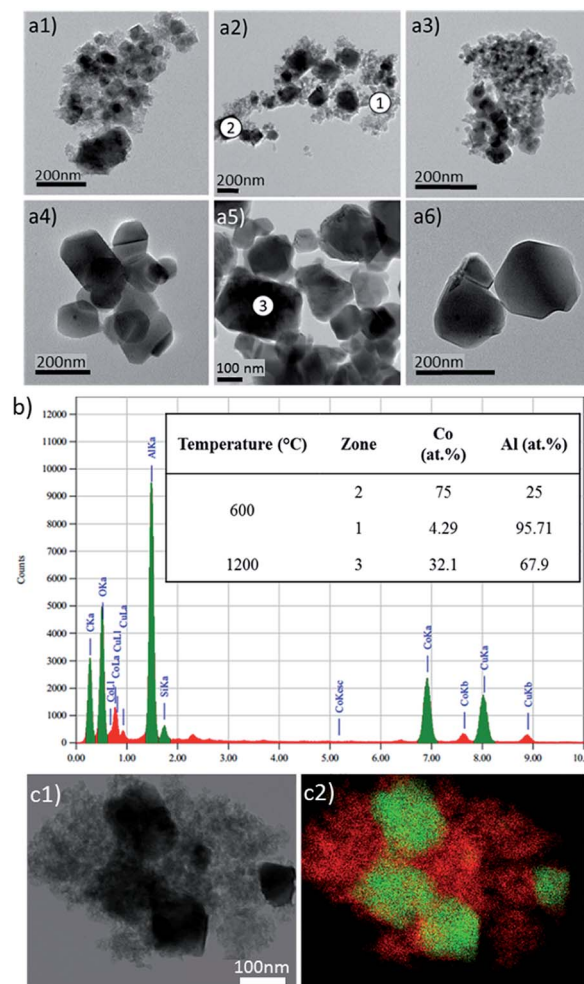


Fig. 2 (a) TEM micrographs of powders calcined at (a1) 400 °C, (a2) 600 °C, (a3) 800 °C, (a4) 1000 °C, (a5) 1200 °C and (a6) 1400 °C. (b) EDX results on the different areas indexed on the micrographs, (c) TEM micrograph (c1) and the corresponding chemical cartography (c2) showing for the 600 °C-annealed compound the non-homogeneous distribution of cobalt and aluminium ions (red colour: Al, green colour: Co).

X-ray diffraction patterns showing pure and single spinel compounds whatever the annealing temperature.

To suppress any ambiguities, deep and accurate analyses using Rietveld refinements were thus made on the X-ray pattern of the different as-prepared samples. Typically, the spinel-type structure adopts the  $Fd\bar{3}m$  space group with  $\text{A}_{1-\xi}^{2+}\text{B}_{\xi}^{3+}[\text{A}_{\xi}^{2+}\text{B}_{2-\xi}^{3+}]\text{O}_4$  composition and distribution,  $\xi$  representing the inversion parameter (the cations inter-brackets correspond to the octahedral sites). The  $\xi$  inversion parameter is so defined as the deviation from the pure direct distribution, *i.e.* with  $\text{A}^{2+}$  ( $\text{Co}^{2+}$ ) cations located into tetrahedral sites only (8a Wyckoff position), and the  $\text{B}^{3+}$  ( $\text{Al}^{3+}$ ) cations consequently located in the octahedral site only (16d Wyckoff position). First, the Rietveld refinements were done in a “standard way”. It means considering a pure phase with  $\text{CoAl}_2\text{O}_4$  with fixed chemical composition but with cobalt/aluminium distribution free to move into the tetrahedral and octahedral sites. In this



refinement process, the  $a$  unit-cell parameter, the peak profile's parameters, the  $(u, u, u)$  oxygen atomic position, and the  $\zeta$  inversion parameter are refined. We decided for all the samples to fix the isotropic displacement factors to  $0.5 \text{ \AA}^2$  for the cations and  $1.0 \text{ \AA}^2$  for the anions, for a better direct comparison. It can be seen from the Rietveld refinement results (reported in Table 1, and Fig. 3a) that, *versus* annealing treatment temperature, an asymptotic decrease of the inversion parameter is observed as an asymptotic increase of the unit-cell parameter. Hence, it would be easily concluded that the evolution of the spinel compound is due to a change of the cationic distribution inside the multi-site spinel network. The negative correlation between the cobalt ion concentration located into octahedral sites and the unit-cell parameters could support the assertion. Also, a slight asymptotic evolution *versus* annealing treatment of the  $(u, u, u)$  free atomic position of the oxygen anions, so directly correlated to the previous evolutions, adds supplementary arguments on the merits of our refinement choices. Secondly, the Rietveld refinements were done in an "exotic way" considering a pure phase with  $\text{Co}_{1+x}\text{Al}_{2-x}\text{O}_4$  chemical composition free to be refined (*via*  $x$  parameter). With this chemical composition, cobalt III is as-created (from electroneutrality law). Also, none vacancies cationic or anionic are created, but in a quite similar manner, it would also be possible to consider some cationic vacancies to simulate the occurrence of  $\text{Co}^{3+}$  ions. In this refinement process, the  $a$  unit-cell parameter, the peak profile's parameters, the  $(u, u, u)$  oxygen atomic position, and the  $x$  cobalt "over-stoichiometry" are the refined parameters (one can note that the same numbers of parameters are refined in first and second refinement processes). As previously, for all the samples, the isotropic displacement factors (Debye–Waller parameters) are fixed to  $0.5 \text{ \AA}^2$  for the cations and  $1.0 \text{ \AA}^2$  for the anions. It can be seen from the Rietveld refinement results (reported in Table 2, Fig. 3b) that, *versus* annealing treatment temperature, an asymptotic decrease of the  $x$  cobalt over-stoichiometry and an asymptotic increase of the unit-cell parameter. One should have to note that in this second hypothesis, the Bragg reliability factor remains rather high (between roughly 10% and 7%) as compared to the first structural hypothesis. However, it is now really doubtful to interpret in a secure manner these results. Indeed, this time, the  $x$  cobalt over-stoichiometry in  $\text{Co}_{1+x}\text{Al}_{2-x}\text{O}_4$  structural hypothesis seems responsible for the colour evolution of the spinel compounds prepared between  $600 \text{ }^\circ\text{C}$  and  $1400 \text{ }^\circ\text{C}$ . In this second model,

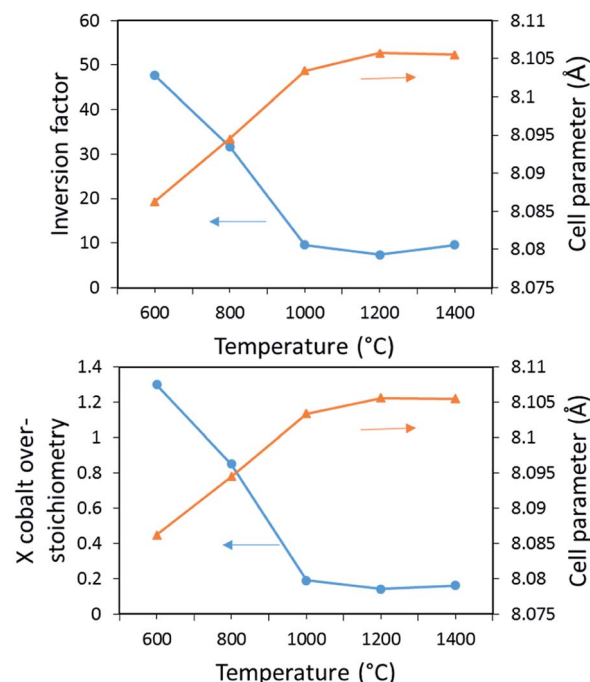


Fig. 3 (Top figure) Unit-cell parameter (▲) and the  $\zeta$  inversion factor (●) in  $\text{Co}_{1-x}\text{Al}_2[\text{Co}_x\text{Al}_{2-x}]\text{O}_4$  compounds issued from the 1<sup>st</sup> refinement process. (Bottom figure) Unit-cell parameter (▲) and  $x$  cobalt over-stoichiometry (●) in  $\text{Co}[\text{Al}_{2-x}\text{Co}_x]\text{O}_4$  compounds issued from the 2<sup>nd</sup> refinement process.

one can assume that the over-stoichiometry ( $x$ ) Co ions adopt also the +III valence states for electroneutrality. Obviously, in the as-prepared compounds the global stoichiometry remains for the Co : Al ratio equal to 1 : 2. Nonetheless, it was evidenced from TEM investigations that cobalt is segregated into the mostly crystallized areas in the low annealed-temperature samples. In the opposite, the aluminium-rich parts of the powder are the badly crystallized parts which do not predominantly affect the X-ray diffraction diagrams. Hence, the experience of an "apparent" over-stoichiometry from Rietveld refinements is not surprising or these latter samples. Moreover, by comparing XRD diagrams of  $\text{CoAl}_2\text{O}_4$ ,  $\text{Co}_2\text{AlO}_4$  and  $\text{Co}_3\text{O}_4$  spinel compounds on Fig. 1-SI,† the unit-cell parameters are very close (see Table 1-SI†) despite the large difference in compositions considering pure  $\text{Co}^{2+}$  phase ( $\text{CoAl}_2\text{O}_4$  annealed

Table 1 Unit-cell parameter,  $u$  oxygen coordinate ( $(u, u, u)$  atomic position), inversion factor  $\zeta$  and reliability factors of  $\text{CoAl}_2\text{O}_4$  compounds prepared from Pechini route followed by post-annealing at several temperatures (1<sup>st</sup> refinement process)

$T$ ( $^\circ\text{C}$ )	$a$ ( $\text{\AA}$ )	$u$	$\zeta$	$R_{\text{Bragg}}$	$R_{\text{f}}$
600	8.0861(5)	0.2609(5)	47.6(1)	3.46	4.20
800	8.0946(5)	0.2631(4)	31.7(1)	1.61	1.85
1000	8.1035(4)	0.2639(4)	9.5(1)	1.30	2.16
1200	8.1057(2)	0.2640(3)	7.3(1)	1.35	1.86
1400	8.1056(3)	0.2640(2)	9.5(1)	1.02	1.50

Table 2 Unit-cell parameter,  $x$  Co over-stoichiometry (in  $\text{Co}_{1+x}\text{Al}_{2-x}\text{O}_4$  model) and reliability factors for  $\text{CoAl}_2\text{O}_4$  compounds prepared from Pechini route followed by post-annealing at several temperatures (2<sup>nd</sup> refinement process)

$T$ ( $^\circ\text{C}$ )	$a$ ( $\text{\AA}$ )	$u$	$x$ Co	$R_{\text{Bragg}}$	$R_{\text{f}}$
600	8.0863(5)	0.2633(6)	1.3(1)	10.1	14.3
800	8.0946(5)	0.2646(5)	0.85(1)	9.1	9.97
1000	8.1035(4)	0.2648(5)	0.19(1)	7.41	11.5
1200	8.1057(3)	0.2639(5)	0.14(1)	6.68	10.9
1400	8.1056(3)	0.2641(5)	0.16(1)	7.21	10.4



at  $T = 1200\text{ }^{\circ}\text{C}$ ) and mixed valences ( $\text{Co}^{2+}/\text{Co}^{3+}$ ) oxides ( $\text{Co}_2\text{AlO}_4$  and  $\text{Co}_3\text{O}_4$ ). It is explained by the very close ionic radii of  $\text{Al}^{3+}$  and  $\text{Co}^{3+}$  (LS) ions. However, one should have to note considering for instance the intensities of (222), (400) and (331) lines, the large difference of (hkl) reticular planes relative intensities showing the partial occupancy of  $\text{Co}^{3+}$  (LS) in octahedral sites.

Consequently, a clear cause of the colour evolution cannot be extracted from Rietveld refinement. The possibility to get as the same time a distribution of both cations (cobalt and aluminium) in both crystallographic sites (octahedral and tetrahedral sites) as well as non-homogeneous distribution of the cations from one crystal to the other (*i.e.* taking into consideration unfixed Co : Al stoichiometry) does not allow the attribution of the colour evolution *versus* annealing temperature. Especially the pattern matching can lead to a very good refinement with the achievement of low correlation factors, using the two tested hypotheses: (i) with a homogeneous chemical composition but with a deviation from a direct spinel structure with an amplitude varying *versus* annealing temperature or (ii) considering a heterogeneous composition (cobalt or aluminium “clustering” respectively for the largest crystals and the smallest crystals) decreasing *versus* temperature to tend to a global homogeneity for the higher temperature.

Anyway, from Pechini process it is not possible to get blue pigments with nanometric crystal size, which is a requirement for valuable applications as mineral pigment incorporated in inks, varnishes or in ceramics. Based on these first analyses, we propose hereafter two ways to prepared nanometric blue cobalt spinels: (i) a top-down approach consisting in a grinding process of the blue powder obtained at high temperatures:  $1400\text{ }^{\circ}\text{C}$ ; (ii) a bottom-up approach, trying to find a chemical synthesis route avoiding the cause of the compound blackening while a low temperature heat treatment is applied. On a more fundamental approach, these two ways are undertaken with the objective to clearly link the spinel blackening to a non-homogeneous cationic distribution or to a consistent inversion parameter in the crystallographic network.

### 3.2. Nano-blue pigments: a top-down approach

A grinding step on the  $1400\text{ }^{\circ}\text{C}$  pigment was carried out thanks to a planetary crusher. The X-ray diffraction patterns of the powder obtained after different milling times are reported on Fig. 4a; corresponding absorbance curves on Fig. 4b and  $L^*a^*b^*$  colours on Fig. 4c. Obviously, the grinding process produces a clear enlargement of the FWHM of the diffraction peaks. The coloration remains bright blue whatever the grinding time. Absorbance curves show that a lightening is quickly obtained (for low grinding time) but this lightening is also rapidly stabilized: the changes observed for prolonged times over 10 minutes are not significant anymore. The slight lightening could come from an increase of the diffusion phenomenon/absorption phenomenon ratio thanks to a disaggregation of the powder and/or a pollution with agate flakes from the crusher and/or the milling balls. This lightening is correlated to a decrease of the d-d absorption band intensities whereas the band position and the bandwidth are not impacted by the grinding step.

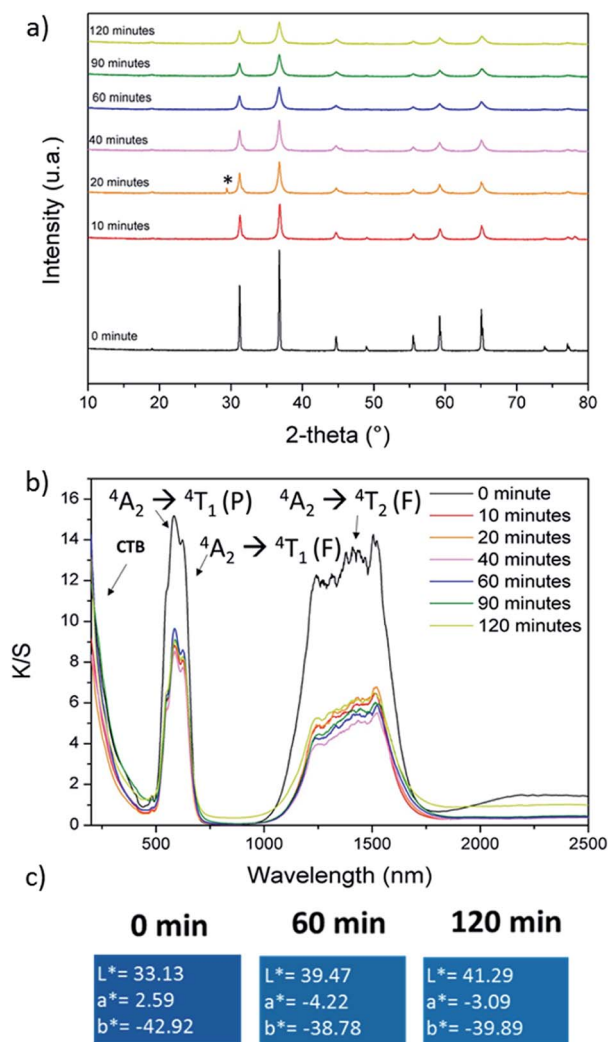


Fig. 4 (a) XRD patterns, (b) K/S spectra and (c)  $L^*a^*b^*$  color parameters of  $\text{CoAl}_2\text{O}_4$  compounds prepared from Pechini route, post annealed at  $1400\text{ }^{\circ}\text{C}$  and subjected to a post-grinding step during several durations.

X-ray diffraction refinements were performed on each pattern. The starting sample, prepared with a post-annealing treatment at  $1400\text{ }^{\circ}\text{C}$  corresponds to a uniform cationic distribution. The Rietveld refinement of the samples subjected to different grinding times was performed considering that the consequence of the grinding can only be an evolution of the inversion parameter and that a segregation of cobalt or aluminium ions cannot occur. Thus, we applied the 1<sup>st</sup> refinement process considering the  $a$  unit-cell parameter, the peak profile's parameters, the  $(u, u, u)$  oxygen atomic position, and the  $\xi$  inversion parameter are free to be refined. As previously, isotropic displacement factors are fixed to  $0.5\text{ \AA}^2$  for the cations and  $1.0\text{ \AA}^2$  for the anions. Debye-Scherrer equation was used to estimate the crystal size evolution. Rietveld refinement results and crystal size extracted from Debye-Scherrer equation are both reported in Table 3. Whatever the grinding time, the unit-cell parameter is unchanged, remaining equal to  $8.105\text{ \AA}$ . The grinding step is associated to a rapid collapse of the crystal size





**Table 3** Unit-cell parameter,  $x$  Co over-stoichiometry and reliability factors  $u$  oxygen coordinate ( $(u, u, u)$ , atomic position), inversion factor  $\zeta$  and reliability factors of  $\text{CoAl}_2\text{O}_4$  compounds prepared from Pechini route, post annealed at  $1400^\circ\text{C}$  and subjected to a post-grinding step during several durations. (1<sup>st</sup> refinement process)

Grind time (min)	$u$	Particle size (nm)	$\zeta$	$R_{\text{Bragg}}$	$R_{\text{f}}$
0	0.2640(2)	89	9.5(1)	1.02	1.50
10	0.2640(5)	35	16.7(1)	8.44	10.5
20	0.2621(5)	36	28.6(1)	8.15	16.1
40	0.2628(5)	31	21.4(1)	8.64	13.0
60	0.2603(6)	25	31.0(1)	8.72	15.7
90	0.2600(5)	25	35.7(1)	9.34	19.5
120	0.2601(5)	25	35.7(1)	6.95	13.3

from about 100 nm to about 35 nm after 10 min grinding. Then the crystal size is stabilized around 30 nm. This first evolution can be directly compared to the colour evolution *versus* grinding time, previously discussed. The colour lightening (evolution of the absorption band intensity) is clearly in perfect agreement with the crystal size. However, the inversion parameter progressively increases *versus* grinding time up to 90 minutes. This inversion parameter is so not directly correlated to the absorption bands intensity. Furthermore, despite the large increase of  $R_{\text{Bragg}}$  reliability factors to 8–6% with the grinding time due to the enlargement of the FWHM of diffraction lines, this experiment proves that the location of cobalt ions in octahedral sites does not bring the detection of new absorption bands. It can be reminded that d–d transitions are still strictly forbidden from Laporte selection rules in centro-symmetric sites as the octahedral ones. Hence, from a fundamental point of view, in  $\text{CoAl}_2\text{O}_4$  compounds, the inversion parameter does not significantly impact the compound's colour. From an applicative point of view, nanometric particles with highly intense blue colour can be obtained from the explored top-down approach: aggressive post-grinding step on a high temperature annealed sample.

A comparison of the signal differences, which are obtained from the three refinement processes we used, is illustrated on the  $800^\circ\text{C}$  annealed samples in Fig. 5 (considering a direct spinel with stoichiometric composition, a spinel with stoichiometric composition and a variable inversion rate parameter, and the over-cobalt stoichiometric compound).

### 3.3. Nano-blue pigments: a bottom-up approach

From the previous experiments, one can conclude that the blackening of the spinel issued from Pechini route and post-annealed at relatively low temperature treatment is caused by the cationic non-homogeneous repartition. One consequence not yet discussed to the segregation in some crystals of a cobalt excess and segregation in some other crystals of aluminium excess is the consequent electronic compensation. Aluminium excess, leading to supplementary “positive charges” in the spinel compounds can be only compensated by the creation of cationic vacancies. This hard compensation is surely at the origin of the low crystallinity of the aluminium-rich parts. On

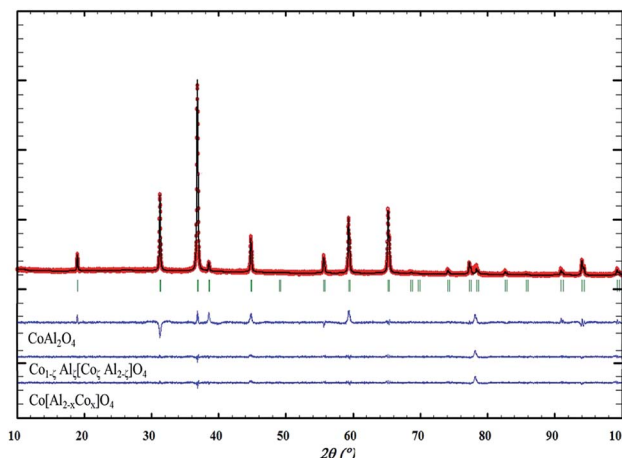


**Fig. 5** XRD experimental, calculated and differential diffractograms using a fixed direct  $\text{CoAl}_2\text{O}_4$  spinel network, partially inverted spinel network, and cobalt overstoichiometric composition.

the other hand, Cobalt excess, leading to a defect of positive charges, can be most easily compensated by the oxidation of a part of the  $\text{Co}^{2+}$  ion into  $\text{Co}^{3+}$  ion. An intervalence charge transfer in the cobalt-rich part should be at the origin of the powder blackening.

The obtaining of a nano-blue pigment with bottom-up approach is so realistic using a synthesis process preventing for cobalt ion oxidation. Unfortunately, for the Pechini sol–gel route we have used, it requires an oxidative post-annealing treatment in order to eliminate the large quantities of carbon groups issued from EG and CA. A coprecipitation process, starting from a mixed solution of  $\text{Al}^{3+}$  and  $\text{Co}^{2+}$  nitrates in stoichiometric proportion on which ammonia was added, was so used ( $\text{pH} = 10$ ). This process leads to a precipitate constituted of a mixture of highly divided  $\text{Co}(\text{OH})_2$  and  $\text{Al}(\text{OH})_3$  phases. Post-annealing treatment can so be performed under argon atmosphere since the reaction between the precursor hydroxides requires only dehydration. X-ray diffraction pattern after an annealing step at  $600^\circ\text{C}$ ,  $700^\circ\text{C}$ ,  $800^\circ\text{C}$  and  $900^\circ\text{C}$  are reported on Fig. 6a. For all the samples, a pure spinel compound as single phase is observed. Nevertheless, as shown by the absorbance spectra and the  $L^*a^*b^*$  colour parameters reported in Fig. 6b and c, respectively, a blackening of the compounds obtained after the lowest annealing treatment temperatures is still observed. It seems that the thermodynamic driving force to get cobalt and aluminium segregation is really important to the detriment of the formation at low temperatures of a single spinel phase. Consequently, even in low oxygen partial pressure atmosphere (the argon flow used exhibits an oxygen partial pressure between  $10^{-4}$  and  $10^{-5}$  atm), cobalt segregation leads to  $\text{Co}^{3+}$  formation and so intervalence phenomenon producing a powder blackening. That is from a negative regard. On the other hand, a blue compound with very interesting colouring parameters can be already achieved using  $900^\circ\text{C}$  as annealing temperature. Furthermore, the  $800^\circ\text{C}$  annealed compound is almost blue with nanosized crystallites. Hence, the synthesis from coprecipitation which allows direct treatments under



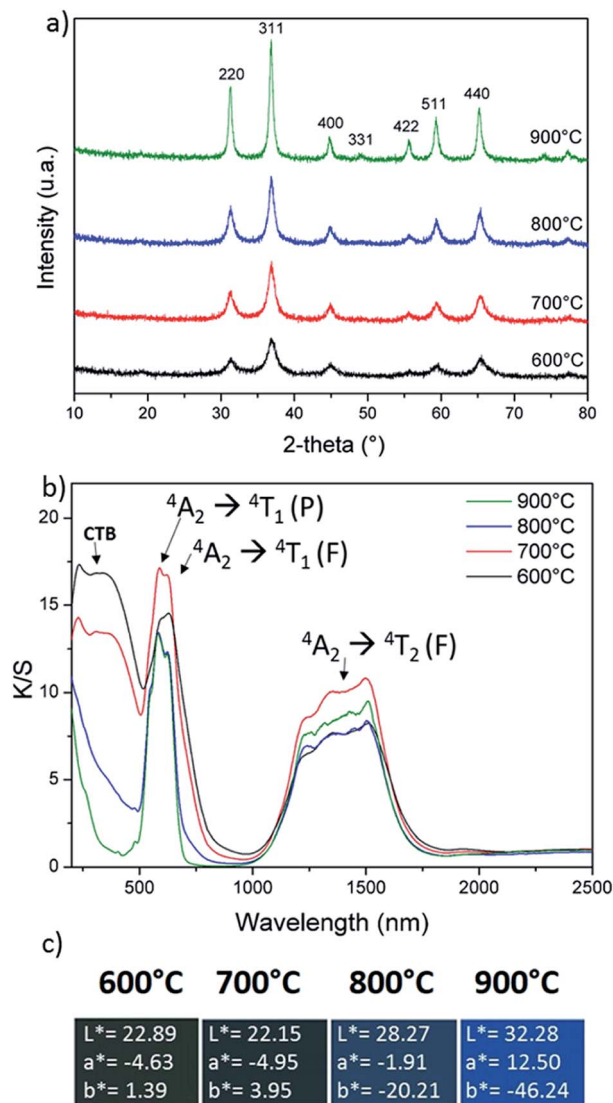


Fig. 6 (a) XRD patterns, (b) K/S spectra and (c)  $L^*a^*b^*$  colour parameters of  $\text{CoAl}_2\text{O}_4$  compounds prepared from a co-precipitation route and post-annealed under argon atmosphere at several temperatures.

argon flow has allowed the obtaining of blue pigment at lowest temperatures. The TEM micrographs reported in Fig. 7 show two important facts: (i) the 600 °C sample is with a narrow distribution crystal size in the contrary to the 600 °C annealed sample issued from Pechini route; (ii) the 900 °C annealed sample is with only 30–40 nm crystal diameter. X-ray diffraction refinement, were performed on each pattern in same condition than previously (Table 4). The inversion factor extracted from these refinements is large in comparison with the samples issued from Pechini route. This shows that despite apparently more homogenous cationic distribution (uniform crystal size is shown on the 600 °C annealed sample), the cationic inversion parameter can still high. At least two sources are at the origin of the inversion parameters: the low crystal size or surface effect (as intrinsic origin), the cobalt – aluminium non-homogeneous distribution (as extrinsic origin). Coprecipitation processes in

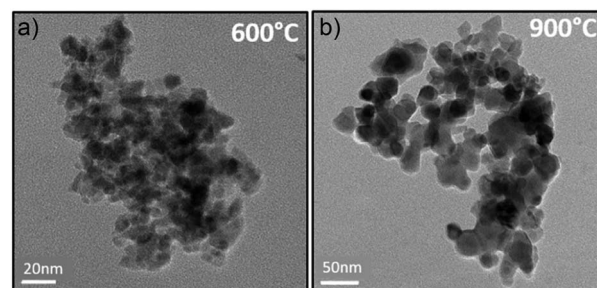


Fig. 7 The TEM micrographs of powders prepared from coprecipitation route and calcined at 600 °C (a) and 900 °C (b) under argon.

comparison to Pechini route leads to better cationic homogeneity but with lower crystal size, comparing two samples with same thermal history.

EELS measurements were undertaken in order to definitively prove that the achievement of more beautiful blue pigments (less blackened) from coprecipitation route than from Pechini route is well due to a lower concentration of  $\text{Co}^{3+}$  ions. EELS spectra of the 600 °C annealed sample issued from Pechini and coprecipitation routes, the 900 °C-annealed sample from coprecipitation and the 1200 °C annealed sample from Pechini routes, are compared on Fig. 8. The spectra analysis was performed with the Digital Micrograph software where the background has been removed and smoothing has been done with Origin software. Theoretical resolution of the machine is 1 eV but for our measurement, the resolution is 1.7 eV due to the thickness of the grains. That is the reason why  $L_3/L_2$  intensity ratios have been discussed instead of the Co  $L_3$  and  $L_2$  lines positions. These values are reported in Table 5.

For comparison the same parameters were extracted from our own observation on  $\text{Co}_3\text{O}_4$  and  $\text{CoO}$  samples, prepared as references. The peak positions are shifted towards low energy *versus* the decrease of the  $\text{Co}^{3+}$  concentration; furthermore, the increase of the  $\text{Co}^{2+}$  content contributes to an enhancement of the  $L_3/L_2$  intensity ratio.<sup>28,29</sup> These two effects are well illustrated comparing the pure  $\text{Co}^{2+}$  oxide ( $\text{CoO}$ ) and the mixed  $\text{Co}^{3+}$ – $\text{Co}^{2+}$  oxide ( $\text{Co}_3\text{O}_4$ ), as references. Clearly, samples prepared from coprecipitation route followed by argon annealing treatment exhibit a significantly lower  $\text{Co}^{3+}$  concentration than the samples prepared from the sol-gel synthesis followed by air annealing treatment. Even, peak positions as well as peak

Table 4 Unit-cell parameter,  $x$  Co over-stoichiometry and reliability factors  $u$  oxygen coordinate ( $(u, u, u)$ , atomic position), inversion factor  $\zeta$  and reliability factors of  $\text{CoAl}_2\text{O}_4$  compounds prepared from a co-precipitation route followed by post-annealing under argon atmosphere at several temperatures. (1st refinement process)

$T$ (°C)	$a$ (Å)	$u$	$\zeta$	$R_{\text{Bragg}}$	$R_{\text{f}}$
600	8.0535(1)	0.2570(7)	50.00(1)	12.1	12.6
700	8.0653(2)	0.2584(5)	30.24(1)	5.09	3.81
800	8.0858(5)	0.2608(4)	29.27(1)	5.60	7.80
900	8.0880(3)	0.2621(4)	21.43(1)	5.29	6.90





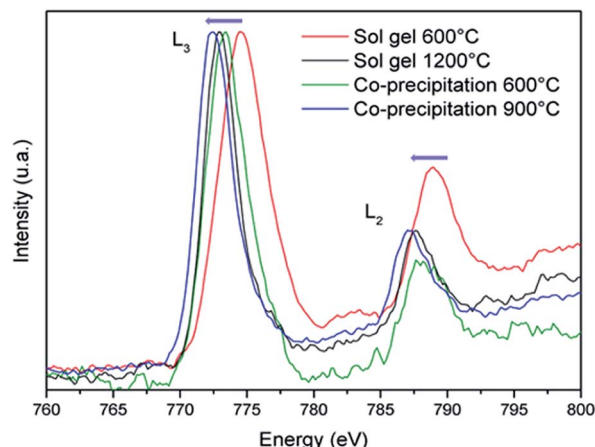


Fig. 8 EELS spectra recorded on  $\text{CoAl}_2\text{O}_4$  compounds synthesized by Pechini and coprecipitation routes with post-annealing treatments at 600 °C or 1200 °C and 600 °C or 900 °C respectively.

intensity ratio indicate that the 900 °C-annealed compound prepared from coprecipitation contains less  $\text{Co}^{3+}$  impurities than the 1200 °C-annealed compound from Pechini process. Definitely, with the aim to prepare nanometric blue pigment with  $\text{CoAl}_2\text{O}_4$  composition, one must avoid  $\text{Co}^{3+}$  formation

Table 5 Ratio intensity, energy resolution and position of the EELS peaks of the spectra recorded on  $\text{CoAl}_2\text{O}_4$  compounds synthesized by Pechini (annealed at 600 °C and 1200 °C) and coprecipitation routes (annealed at 600 °C and 900 °C).  $\text{Co}_3\text{O}_4$  and  $\text{CoO}$  oxides prepared at 600 °C and 900 °C, respectively have been reported as comparison

Synthesis route	$T$ (°C)	Res. (eV)	Co $L_3$ (eV)	Co $L_2$ (eV)	$I(L_3/L_2)$
$\text{Co}_3\text{O}_4$ reference	600	1.71	774.2	788.4	1.63
$\text{CoO}$ reference	900	1.54	772.8	788.0	3.07
Sol-gel	600	2.1	774.0	789.0	2.24
Sol-gel	1200	1.71	773.0	788.0	2.70
Co-precipitation	600	2.3	773.4	788.5	2.41
Co-precipitation	900	2.3	772.5	787.2	3.00

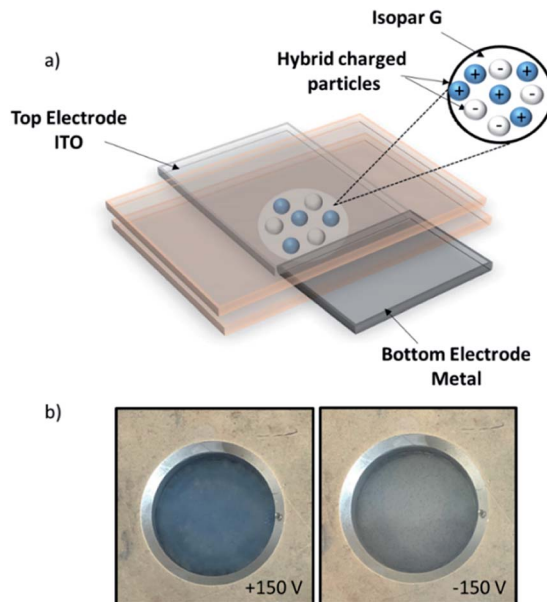


Fig. 9 (a) Scheme of the dual-colour display, (b) photographs (top views) of the dual-colour display under  $\pm 150$  V.

using some “soft chemistry” synthesis routes allowing the use of low oxygen partial pressure annealing treatments.

### 3.4. Formulation of hybrid particles, application in electrophoretic displays

$\text{CoAl}_2\text{O}_4$  milled pigments have been modified by silanisation with various *n*-trimethoxysilanes (OTS, DTS, HDTS) in dry toluene to improve their dispersion into nonpolar solvent (Fig. SI-2).<sup>†</sup> Then dispersion polymerization with methyl-metacrylate in Isopar G has been done to obtain stable charged hybrid.<sup>23,24</sup> For the polymerization step, two parameters have been varied: the length of the macro-initiator (Lauryl acrylate 4500 or 21 000  $\text{g mol}^{-1}$ , hereafter noted Ma)<sup>21</sup> and the volume of the liquid monomer (0.5 or 1 mL). The various physical properties of the as-prepared inks are all grouped in the Table SI-2.<sup>†</sup> The stability of the obtained inks was evaluated thanks to (i) an

Table 6 Experimental conditions and characteristics for the silanization and polymerisation of the  $\text{CoAl}_2\text{O}_4$  and  $\text{TiO}_2$  pigments

Silanization					
Pigment	Modifier + $V_{\text{modifier}}$ v/v%	Solvent + volume (mL)	[Pigment] $\text{g L}^{-1}$	Particle diameter (nm)	Electrophoretic mobility ( $10^4 \mu\text{m}^2 \text{Vs}^{-1}$ )
$\text{CoAl}_2\text{O}_4$ -5OTS	5 OTS	10 mL toluene	32.20	281	−0.176
$\text{TiO}_2$ -1OTS	1 OTS	90 mL toluene	50.00	59	−0.012
Dispersion polymerisation					
Hybrid	Monomer + [monomer] ( $\text{mol L}^{-1}$ )	[MA(La)] ( $\text{mmol L}^{-1}$ )	[Pigment] $\text{g L}^{-1}$	Particle diameter (nm)	Electrophoretic mobility ( $10^4 \mu\text{m}^2 \text{Vs}^{-1}$ )
$\text{CoAl}_2\text{O}_4$ -5OTS-MMA	0.94 MMA	2.67	15.31	595	+0.070
$\text{TiO}_2$ -1OTS-Sty	0.91 styrene	2.27	10.70	533	−0.656



indirect quantification of the sedimentation state from Turbiscan analysis: lower is the TSI (Turbiscan Stability Index) and more stable is the hybrid dispersion (Fig. SI-3†), (ii) a qualitative estimation of the sedimentation state from the observation of the as-prepared inks (Fig. SI-4†). The different hybrid particles were observed by TEM instrument (Fig. SI-5,† for illustration). Blue hybrid particles were mixed with TiO<sub>2</sub> hybrid dispersions in the proportion 1 : 4 without any charge control agent. To ensure the stability of the inks, macro-initiator has been used during the polymerisation. Blue and white hybrid particles exhibit opposite charges, whereas their isoelectric point are quite similar (IEP<sub>CoAl<sub>2</sub>O<sub>4</sub></sub> = 5.1 and IEP<sub>TiO<sub>2</sub>, anatase</sub> = 3.4). Actually, the surface charge has been partially brought by the monomer used during the polymerisation. As described previously, CoAl<sub>2</sub>O<sub>4</sub> pigments have been modified with OTS and polymerised with MMA whereas TiO<sub>2</sub> (anatase) pigments have been modified with OTS and polymerised with styrene. Characteristics of these dispersions are reported in Table 6.

Detailed description of the complex optimization of the formulation process of such inks will be described in a further publication. Finally, these two-coloured dispersions have been tested into an electrophoretic test-cell (dual colour display) to observe a contrast between blue and white hybrids on the top surface of the cell. The display is composed of two electrodes, one transparent electrode on the top (ITO glass) and one reflective electrode on the bottom (metal). After the introduction of the inks into this device, a potential difference of  $\pm 150$  V was applied. White particles which are negatively charged migrate to the top electrode when a negative voltage is applied whereas blue particles migrate when a positive voltage is applied (Fig. 9).

## 4. Conclusion

With the objective, to get nanosized blue inorganic pigment to be incorporated in inks for instance, our investigation showed that the blackening of 'CoAl<sub>2</sub>O<sub>4</sub>' blue pigment is related to the oxidation of Co<sup>2+</sup> into Co<sup>3+</sup> (LS) and the stabilization of trivalent cobalt in octahedral site in substitution of Al<sup>3+</sup> ions. Thanks to a bottom-up and top-down approaches, it has been first demonstrated that the inversion rate in this spinel network by keeping the same oxidation of cobalt (Co<sup>2+</sup>), cannot explained the blackening of the inorganic pigment. Furthermore, by a simple coprecipitation of Al/Co nitrates in basic medium followed by annealing under Ar, a strong blue pigment can be obtained at medium temperature, *i.e.* 900 °C with nanosized particles around 30–40 nm. The control of the cobalt oxidation state in this blue pigment is a crucial point which can be achieved by maintaining a low partial pressure of oxygen at low temperature in order to get nanosized inorganic particles. Thanks to a complete structural analysis of cobalt blue spinel, the origin of blackening has been fully understood and new solutions have been proposed.

In a last part, CoAl<sub>2</sub>O<sub>4</sub> milled pigments have been modified to formulate electrophoretic inks. An electrophoretic display was filled with blue hybrids mixed with TiO<sub>2</sub> hybrid in order to obtain a dual-color contrast.

## Author contributions

The manuscript was written through contributions of all authors.

## Conflicts of interest

There are no conflicts to declare.

## References

- 1 M. Dondi, F. Matteucci, G. Baldi, A. Barzanti, G. Cruciani, I. Zama and C. L. Bianchi, *Dyes Pigm.*, 2008, **76**(1), 179–186.
- 2 K. H. Hudson Winbow and J. T. Cowley, *Ceram. Eng. Sci. Proc.*, 1996, **17**(1), 167–172.
- 3 R. K. Mason, *Am. Ceram. Soc. Bull.*, 1961, **40**(1), 5–6.
- 4 S. Meseguer, M. A. Tena, C. Gargori, J. A. Badenes, M. Llusar and G. Monrós, *Ceram. Int.*, 2007, **33**(5), 843–849.
- 5 R. O. Kuzian, A. M. Daré, P. Sati and R. Hayn, *Phys. Rev. B: Condens. Matter Mater. Phys.*, 2006, **74**, 155201.
- 6 J. M. Rojo, J. L. Mesa, J. L. Pizarro, L. Lezama, M. I. Arriortua and T. Rojo, *J. Solid State Chem.*, 1997, **132**, 107–112.
- 7 C. Angeletti, F. Pepe and P. J. Porta, *J. Chem. Soc.*, 1977, **73**(12), 1972–1982.
- 8 M. Zayat and D. Levy, *Chem. Mater.*, 2000, **12**(9), 2763–2769.
- 9 P. G. Casadoa and I. Rasines, *J. Solid State Chem.*, 1984, **52**(2), 187–190.
- 10 R. Pozas, V. M. Orera and M. Ocaña, *J. Eur. Ceram. Soc.*, 2005, **25**(13), 3165–3172.
- 11 G. Monari and T. Manfredini, *Ceramic engineering & science proceedings*, The american ceramic society, 1996, vol. 1, pp. 167–172.
- 12 W. Li, J. Li and J. Guo, *J. Eur. Ceram. Soc.*, 2003, **23**(13), 2289–2295.
- 13 D. M. A. Melo, J. D. Cunha, J. D. G. Fernandes, M. I. Bernardi, M. A. F. Melo and A. E. Martinelli, *Mater. Res. Bull.*, 2003, **38**(9–10), 1559–1564.
- 14 N. Ouahdi, S. Guillemet, J. J. Demai, B. Durand, L. Er Rakho, R. Moussa and A. Samedi, *Mater. Lett.*, 2005, **59**(2–3), 334–340.
- 15 C. Wang, S. Liu, L. Liu and X. Bai, *Mater. Chem. Phys.*, 2006, **96**(2–3), 361–370.
- 16 S. Kurajica, J. Popović, E. Tkalčec, B. Gržeta and V. Mandić, *Mater. Chem. Phys.*, 2012, **135**(2–3), 587–593.
- 17 H. S. C. O'Neill, *Eur. J. Mineral.*, 1994, **6**(5), 603–610.
- 18 A. Nakatsuka, Y. Ikeda, Y. Yamasaki, N. Nakayama and T. C. Mizota, *Solid State Commun.*, 2003, **128**(2–3), 85–90.
- 19 S. Salem, *J. Ind. Eng. Chem.*, 2014, **20**(3), 818–823.
- 20 R. Franco, F. Tielens, M. Calatayud and J. M. Recio, *High Pressure Res.*, 2008, **28**(4), 521–524.
- 21 J. Merikhi, H.-O. Jungk and C. Feldmann, *J. Mater. Chem.*, 2000, **10**, 1311–1314.
- 22 M. Pechini, *US Pat.* 3330697, 1967.
- 23 A. Noël, D. Mirbel, A. Charbonnier, E. Cloutet, G. Hadzioannou and C. Brochon, *J. Polym. Sci., Part A: Polym. Chem.*, 2017, **55**(2), 338–348.



- 24 A. Noel, D. Mirbel, E. Cloutet, G. Fleury, C. Schatz, C. Navarro, G. Hadziioannou and C. Brochon, *Appl. Surf. Sci.*, 2018, **428**, 870–876.
- 25 J. Rodriguez-Carvajal, *Commission on Powder Diffraction (IUCr)*, 2001.
- 26 A. Boultif and D. Louer, *J. Appl. Crystallogr.*, 2004, **37**, 724–731.
- 27 M. Gaudon, A. Apeceixborde, M. Ménétrier, A. Le Nestour and A. Demourgues, *Inorg. Chem.*, 2009, **48**(19), 9085–9091.
- 28 T. Yamaguchi, S. Shibuya, S. Suga and S. J. Shin, *J. Phys. C: Solid State Phys.*, 1982, **15**(12), 2641.
- 29 Z. L. Wang, J. S. Yin and Y. D. Jiang, *Micron*, 2000, **31**(5), 571–580.

